ACS APPLIED MATERIALS & INTERFACES

Research Article

Cite This: ACS Appl. Mater. Interfaces 2018, 10, 43211−43218

www.acsami.org

Understanding Electric Double-Layer Gating Based on Ionic Liquids: from Nanoscale to Macroscale

Wei Zhao,[†,▽] Sheng Bi,[†,▽] Nina Balke,[‡] Philip D. Rack,[‡,⊥] Thomas Zac Ward,[§] Sergei V. Kalinin,[‡] Sheng Dai,[∥,#] and Guang Feng[†,*]

[†]State Key Laboratory of Coal Combustion, School of Energy and Power Engineering, Huazhong University of Science and Technology, Wuhan 430074, China

[‡]Center for Nanophase Materials Sciences, [§]Materials Science and Technology Division, and [∥]Chemical Sciences Division, Oak Ridge National Laboratory, Oak Ridge, Tennessee 37831, United States

[⊥]Department of Materials Science and Engineering and [#]Department of Chemistry, University of Tennessee, Knoxville, Tennessee 37996, United States

Supporting Information

ABSTRACT: In electric double-layer transistors (EDLTs), it is well known that the EDL formed by ionic liquids (ILs) can induce an ultrahigh carrier density at the semiconductor surface, compared to solid dielectric. However, the mechanism of device performance is still not fully understood, especially at a molecular level. Here, we evaluate the gating performance of amorphous indium gallium zinc oxide (a-IGZO) transistor coupled with a series of imidazolium-based ILs, using an approach combining of molecular dynamics simulation and finite element modeling. Results reveal that the EDL with different ion structures could produce inhomogeneous electric fields at the solid−electrolyte interface, and the heterogeneity of electric field-induced charge distributions at semiconductor surface could reduce the electrical conductance of a-IGZO during gating process. Meanwhile, a resistance network analysis was adopted to bridge the nanoscopic data with the macroscopic transfer characteristics of IL-gated transistor, and showed that our theoretical results could well estimate the gating performance of practical devices. Thereby, our findings could provide both new concepts and modeling techniques for IL-gated transistors.

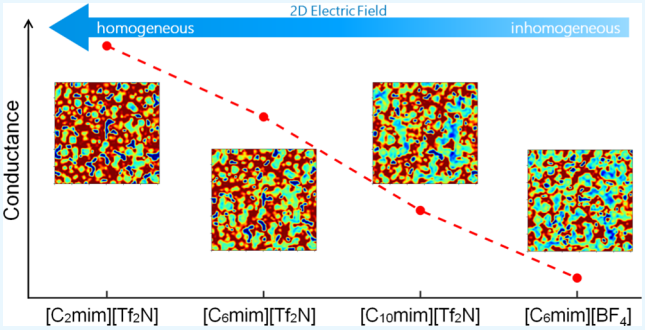

KEYWORDS: *electric double-layer transistor, liquid gating effect, ionic liquid, amorphous indium gallium zinc oxide, surface charge homogeneity*

INTRODUCTION

Liquid electrolytes have been widely used as the dielectric materials in electric double-layer transistors (EDLTs) to tune the electrical properties of various materials over the past years.[1−8] Owing to the ultrathin thickness, EDLs could achieve extremely high capacitance and interfacial electric fields at liquid−solid interface. Hence, these devices can accomplish a large carrier density (up to 10^{22} cm^{-3})[7] under a much lower gate voltage than conventional field-effect transistors (FETs). Among a variety of liquid electrolytes, ionic liquids (ILs) have attracted great attention due to their superior thermal and chemical stability and wide electrochemical window. These properties could contribute to broad working scope, fast switching, and stable device performance.[5−7] For instance, by employing ionic liquids as the gate dielectrics, the metal−insulator transition can be well controlled in metal oxides, such as $NdNiO_3$, $SrTiO_3$, $KTaO_3$, and $La_{2-x}Sr_xCuO_4$, since the ultrahigh interfacial capacitance can yield a large carrier density compared with conventional gate dielectric.[4,9−13] Benefiting from the ultralarge localized electric field formed by EDL, these metal oxides have also achieved transition to superconductivity. Furthermore, it was also reported that coupled with ionic liquid, the carrier mobility of two-dimensional (2D) materials can be significantly improved.[14,15] The ultrathin ionic liquid layer formed between the semiconductor and source−drain electrode could also reduce the Schottky barrier via strong band bending and finally result in a low-resistance ohmic contact. In particular, IL-gated amorphous metal-oxide films could exhibit excellent transistor properties with field-effect carrier mobility over 20 cm^2/V s as well as the threshold voltage and subthreshold swing less than 0.5 V and 0.1 V/dec, respectively.[16−18] Overall, IL can yield higher on-current and lower switching voltage, which makes it a versatile tool to tune the transistor properties in EDLTs.

Among various liquid gate dielectrics, it has been experimentally shown that during the gating process, the

Received: September 2, 2018
Accepted: November 13, 2018
Published: November 13, 2018

DOI: 10.1021/acsami.8b15199
ACS Appl. Mater. Interfaces 2018, 10, 43211−43218

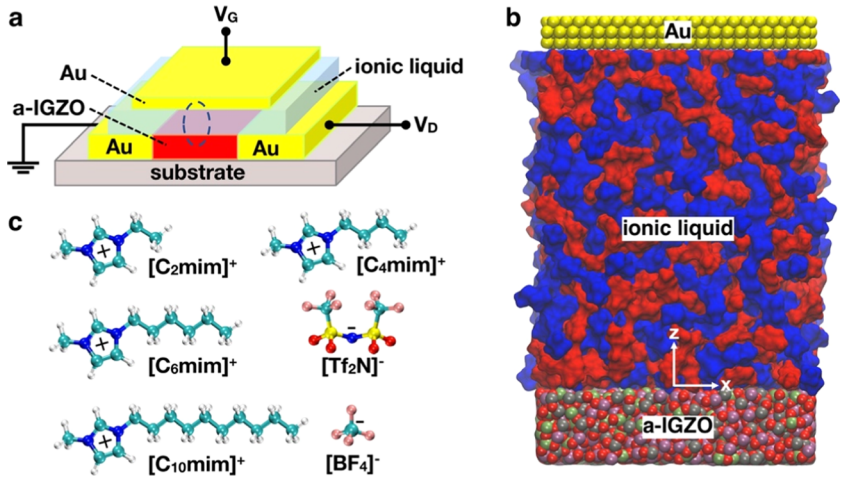

Figure 1. Schematics of IL-gated transistors and corresponding MD simulation. (a) Schematic diagram of an IL-gated transistor. The blue dash ellipse shows the target area for molecular modeling. (b) Snapshot of MD simulation. $z = 0$ corresponds to a-IGZO surface. The red and blue spheres between Au and a-IGZO stand for cation and anion of ILs, respectively. (c) All-atom models of ions in ILs used in this work.

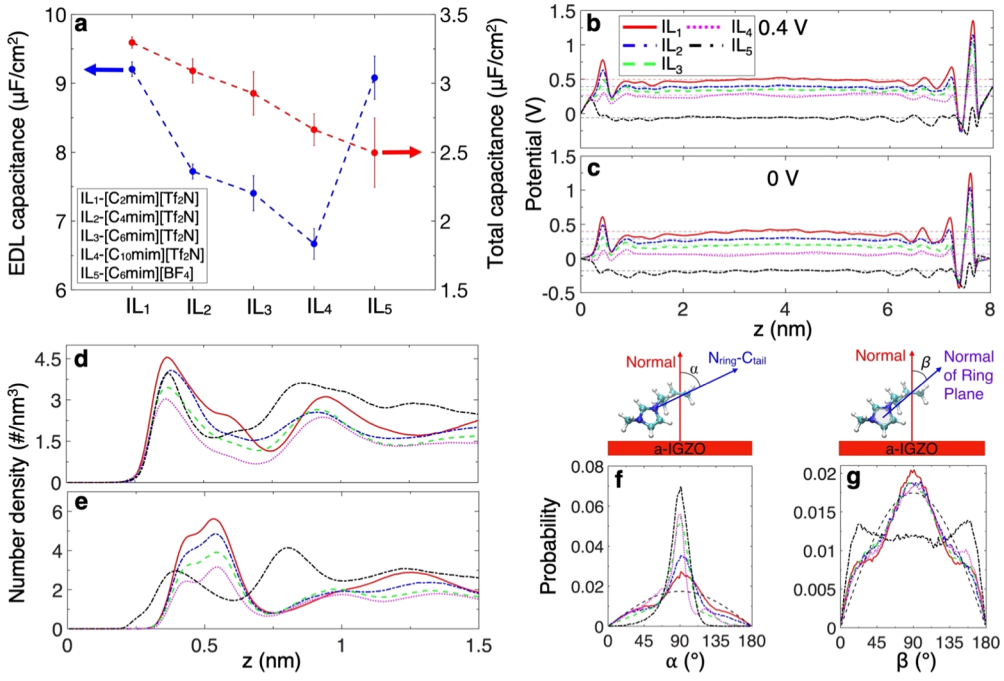

Figure 2. EDL capacitance and EDL structure with different ILs. (a) EDL (a-IGZO side) and total capacitances vary with different ILs. (b, c) Electrical potential distributions across the whole channel under gate voltages of 0.4 V (b) and 0 V (c). (d, e) Number densities of cations (d) and anions (e) as a function of distance from a-IGZO with a gate voltage of 0.4 V. (f–g) Orientation distributions of alkyl tail (f) and imidazolium ring (g) in the first cation layer at a-IGZO under a gate voltage of 0.4 V.

gating performance, including ON/OFF ratio, threshold voltage, source–drain current, and transistor mobility, strongly correlates with the capacitance.[19−23] As for ILs, many experimental and modeling studies have reported that different ILs could render different capacitances at solid–IL interfaces, and the EDL capacitance depends highly on the ion size.[24−28] Thus, it could be reasonable to procure better transistor properties (such as higher ON-current) if adopting the IL supplying a larger EDL capacitance.[29] Beyond the high capacity of IL-based EDLs, researches have pointed out that the IL ions localized at semiconductor surface could hinder the carrier hopping, resulting in reduced carrier mobility.[30,31] Therefore, the induced carriers and their inhomogeneous distribution, originating from disordered electric fields derived by ions in EDLs,[32,33] should be indispensably explored in electrolyte-gating studies. However, the ion size effect on capacitance was mainly analyzed for charge-storage devices (in particular the modeling work focused on ideal solid surfaces),[24−27] and the impact of carrier distribution on gating performance was only investigated by experiments, which mainly focused on the ion behaviors in EDL.[34,35] Thus, revealing the effects of different ILs on EDL capacitance at non-atomic-flat semiconductor surface during gating process and carrier distribution at semiconductor surface from molecular level as well as bridging these nanoscale features with macroscale gating performance is of great importance for the design and optimization of IL-gated FETs.

DOI: 10.1021/acsami.8b15199
ACS Appl. Mater. Interfaces 2018, 10, 43211−43218

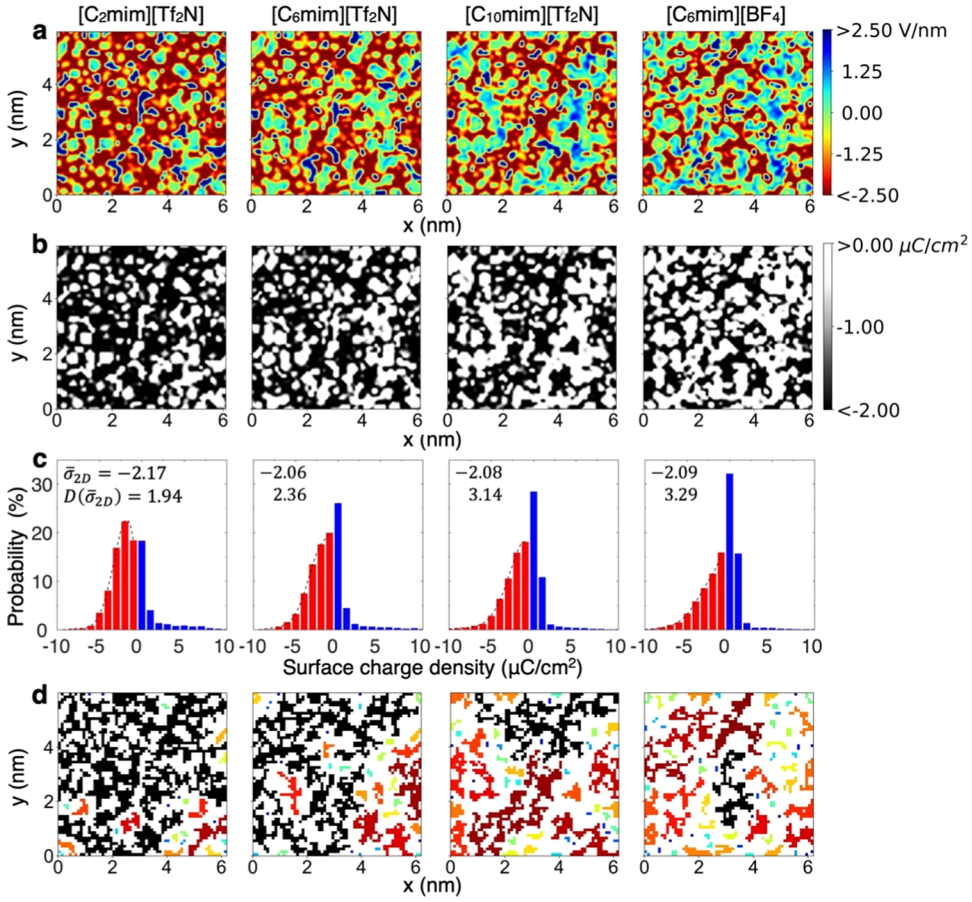

Figure 3. Homogeneity analyses of charge distribution. Electric field distributions (a), 2D surface charge density (σ_{2D}) distribution at the a-IGZO surface (b), probability distribution of 2D surface charge densities (c), and percolation visualizations (d) at a-IGZO surface vary with different ILs under the gate voltage of 0.4 V. For electric field distributions (a), the red zones denote negative values means that the negative electrical fields pointing toward opposite *z*-direction, which could gather electrons on the a-IGZO surface of the liquid−solid interface and turn electron-aggregate areas into conducting regions, and the blue zones correspond to insulating regions in the contrary. In probability distribution of 2D surface charge densities (c), the red zones are negative charged regions (conducting regions), whereas the blue zones are positive charged regions (insulating regions). Averaged surface charge density ($\bar{\sigma}_{2D}$) and corresponding variance ($D(\bar{\sigma}_{2D})$) for conducting regions were calculated and are shown in (c). The different colored regions in (d) represent different charge clusters in "ON" state, and the biggest charge cluster is shown in black; all of the "OFF" state regions are shown in white.

In this work, we systematically investigated EDLs formed by ILs at an amorphous indium gallium zinc oxide (a-IGZO) semiconductor surface, using hierarchical simulations. To explore the impact of ion size and type on gating performance, ILs are selected with different cations and anions, i.e., 1-*n*-3-methylimidazolium bis(trifluoromethylsulfonyl)imide ($[C_nmim][Tf_2N]$, n = 2, 4, 6, 10) with different alkyl chain lengths and 1-hexyl-3-methylimidazolium tetrafluoroborate ($[C_6mim][BF_4]$). The hierarchical simulations presented here include molecular dynamics (MD) simulations for interfaces of ILs and a-IGZO at atomistic level and finite element modeling (FEM) for the resistance network analysis at macroscopic level. Specifically, the structure with EDL capacitance of each IL near a-IGZO is illustrated to reveal the ion size/type effects by MD simulation. Then, utilizing 2D surface charge density and distribution obtained from MD simulation as inputs for the finite element analysis, we quantitatively assess the influence of the heterogeneity of surface charge distribution on the conductance and carrier mobility of a-IGZO.

RESULTS AND DISCUSSION

To mimic an IL-gated transistor (Figure 1a), a typical channel-like simulation cell is used, which consists of ionic liquids sandwiched by gold (as the gate metal) and a-IGZO (Figure 1b). The amorphous phase of the IGZO material is obtained through quenched molecular dynamics (QMD) simulation from the crystalline phase, in line with experiments.[36,37] Five types of ILs, $[C_nmim][Tf_2N]$ (n = 2, 4, 6, 10) and $[C_6mim][BF_4]$, are selected to examine the effects of capacitance and charge distribution on performance of IL-gated transistor (Figure 1c).

We begin our work by scrutinizing how alkyl chain length and anion type affect the EDL capacitance at both the a-IGZO side and the gate side (hereafter termed as a-IGZO side capacitance and gate side capacitance, respectively). The EDL capacitance could be computed by $C_{EDL} = \frac{\sigma}{\phi_{EDL}}$, where σ is the charge density at a-IGZO/gate surface, ϕ_{EDL} is the potential drop across the EDL relative to its value at potential of zero charge (PZC) of the electrode, i.e., $\phi_{EDL} = (\phi_{electrode} - \phi_{bulk}) - (\phi_{electrode} - \phi_{bulk})|_{PZC}$. As shown in Figure 2a, we find that for ILs with the same anion, the a-IGZO side capacitance

DOI: 10.1021/acsami.8b15199
ACS Appl. Mater. Interfaces 2018, 10, 43211−43218

decreases with the cation alkyl chain increasing from ethyl to decyl (i.e., cation changes from $[C_2mim]^+$ to $[C_{10}mim]^+$), which matches the previous work on other electrodes.[24,25,27] For the ILs with the same cation, the larger anion $[Tf_2N]^-$ leads to a lower a-IGZO side capacitance, in accordance with reported studies that ILs with bigger ion size could result in lower EDL capacitances (in those studies, they all used three-electrode system to measure the differential capacitance[24,25,28,38]). However, the total capacitance (two sides capacitance in series) of $[C_6mim][Tf_2N]$ is higher than that of $[C_6mim][BF_4]$. From Figure 2b,c, it can be seen that the potential distribution across the cell of $[C_6mim][BF_4]$ differs a lot from that of other ILs due to the very different anion. When a gate voltage of 0.4 V was applied (Figure 2b), using IL $[C_6mim][BF_4]$ ϕ_{EDL} at a-IGZO side is much smaller than the gate side (0.12 vs 0.28 V), indicating a smaller gate side capacitance than a-IGZO side capacitance. Moreover, IL $[C_6mim][BF_4]$ shows a positive value of PZC, whereas all $[Tf_2N]^-$-based ILs have negative values (Figure 2c), which also contributes to the larger a-IGZO side capacitance than its counterpart of IL $[C_6mim][Tf_2N]$. These results designate that the alkyl chain length of cation and the type of anion both have direct impact on the a-IGZO side capacitance, and anion type affects the gate side capacitance significantly (Figure S4).

The nature of these findings could be rationalized by the detailed structure of interfacial ILs, which could be characterized by the density and orientation distributions of electrolyte ions near a-IGZO and gold surfaces. Specifically, when applying a gate voltage of 0.4 V, we observe that for ILs $[C_nmim][Tf_2N]$ (n = 2, 4, 6, 10), alternating layers of cations and anions are formed near the negatively electrified a-IGZO surface, and the first cation layer is closer to a-IGZO than anion layers (Figure 2d,e). As the alkyl chain length increases, the peak locations of ion distributions vary little, however, the ion peak height decreases obviously. The packing of interfacial cations also lines up with their orientations (Figure 2f,g; IL_{1-4}). For $[Tf_2N]^-$-based ILs, the alkyl chain of cation tends to be parallel to the a-IGZO surface as the chain length increases while the influence of chain length on the orientation of imidazolium ring is minor. Thus, the lying flat of alkyl chain would reduce the space to accommodate more cation rings near a-IGZO surface (note that the charge is mostly concentrated on the ring), potentially leading to less net charge at a-IGZO surface and embodying smaller EDL capacitance. When the anion is changed to $[BF_4]^-$, the first anion-adsorbed layer of $[C_6mim][BF_4]$ is found to be closer to the a-IGZO surface due to its smaller anion size than $[Tf_2N]^-$ (Figure 2e; IL_5). Due to $[BF_4]^-$ closer to a-IGZO surface leaving more space, the imidazolium ring of cation would orient more parallel to a-IGZO surface (Figure 2f,g; IL_5), facilitating to reduce the EDL thickness as well as increase EDL capacitance. Nonetheless, the total capacitance of the cell using IL $[C_6mim][BF_4]$ as a dielectric is small. This could be attributed to quite low gate side capacitance of $[C_6mim][BF_4]$ (Figure S4), as $[Tf_2N]^-$ reorients its structure and makes the charge on ions closer to the gate than $[BF_4]^-$ even though $[BF_4]^-$ has smaller size.

Generally, larger EDL capacitance could enhance charge density at the semiconductor surface as well as gating performance. However, previous experimental studies on IL-gated transistors postulated that the electrical conductance of the conduction path(s) on semiconductor surface could be reduced due to the inhomogeneous electric fields resulting in localization of some of the carriers.[30,31] Indeed, the in-plane distribution and orientation of the electrolyte ions could induce disordered electric fields at the semiconductor surface in EDLTs. Figure 3a exhibits MD-obtained 2D electric field distributions at a-IGZO surface contacting with different ILs, and highly heterogeneous electric fields are observed at a-IGZO surface, which generate inhomogeneous charge density distributions at a-IGZO surface (Figures 3b,c and S3−S5). Since the a-IGZO acts as a n-channel semiconductor, here we mainly focus on the negative charges as carriers in the following analyses.[39]

Specifically, for ILs $[C_nmim][Tf_2N]$ (n = 2, 6, 10), the regions with negative electric fields, which would drive charges to accumulate on the a-IGZO surface contacting with ILs, named conducting regions, shrink and scatter as the alkyl chain length increases, and IL $[C_6mim][BF_4]$ seems to produce the most heterogeneous electric field distribution (Figure 3a). Originating from local electric fields induced by disordered cations/anions in EDLs at a-IGZO, the 2D charge densities at a-IGZO surface (σ_{2D}), shown in Figure 3b, are heterogeneously elicited and localized as well, following the same trends as electric fields. It exhibits that with the cation size getting smaller, more black zones (with high electron density) appear at a-IGZO surface and gradually join together. The effect of gate voltage magnitude on σ_{2D} is also analyzed in Part 5 of Supporting Information. We further illustrate and quantitatively evaluate surface charge localizations by their histograms and calculating the variance $D(\overline{\sigma}_{2D})$ of 2D surface charge densities for conducting regions with respect to the averaged values ($\overline{\sigma}_{2D}$) (Figure 3c, the upper left corner of each subgraph). It can be observed that for ILs $[C_nmim][Tf_2N]$ (n = 2, 6, 10), the 2D charge densities on a-IGZO surface are spread farther from their average value with increasing the alkyl chain length, and IL $[C_6mim][BF_4]$ exhibits the widest range of charge distribution. This is because the first layer of $[BF_4]^-$ is closer to electrified a-IGZO surface than $[Tf_2N]^-$ (Figure 2e), which would weaken the negative electric fields or even generate positive electric fields, resulting in more inhomogeneous charge distributions at a-IGZO surface.

To delve deeper into how the heterogeneity of charge distribution impacts the transfer characteristics (e.g., transition between the "ON" and "OFF" states) of a-IGZO gated by the studied ILs, we first use the percolation model[31] to find whether there are conduction paths for possible electron transfer at the a-IGZO surface. On the basis of the local charge density distribution (Figure 3b), each grid (size: 0.1 nm × 0.1 nm) on a-IGZO surface was labeled by "ON" state or OFF state with a threshold charge density of −2.00 $\mu C/cm^2$, which corresponds to the average charge density of conducting regions (Figure 3c). Herein, the grids with "ON" state (where $\overline{\sigma}_{2D} < -2.00\ \mu C/cm^2$) were grouped into different clusters based on the connectivity of the local charges. Specifically, the local charge that connects with each other (in other word, whether one charge could find a neighboring free site) would form a charge cluster. More details of this method are described in Part 6 of Supporting Information. From Figure 3d, one could see that for IL $[C_2mim][Tf_2N]$, most of the charges are connected to form a large charge cluster (in which conduction paths exist) that dominates the a-IGZO surface. With increasing the alkyl chain length, the area of the biggest charge cluster dwindles, whereas smaller charge clusters are formed, but disconnected and scattered at the a-IGZO surface. For IL $[C_{10}mim][Tf_2N]$, the largest charge cluster cannot

DOI: 10.1021/acsami.8b15199
ACS Appl. Mater. Interfaces 2018, 10, 43211−43218

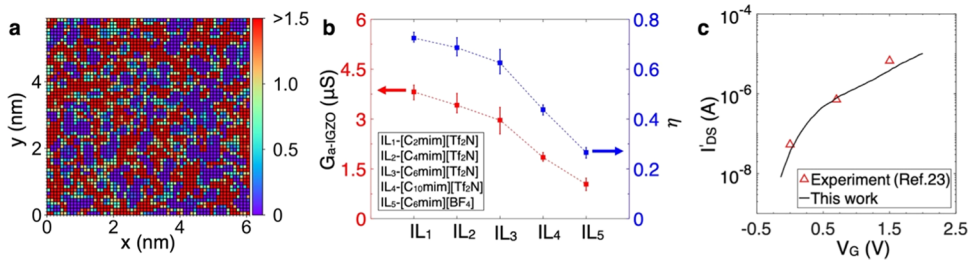

Figure 4. Quantitative analyses of gating effects. (a) Electrical conductance (G) of each grid on uniform meshes of a-IGZO surface in FEM analysis (the values have been magnified 10^5 times, unit: S) of a-IGZO. (b) Equivalent conductance ($G_{a\text{-IGZO}}$) and homogeneity degree (η) with different ILs under a gate voltage of 0.4 V. (c) The equivalent currents (I'_{DS} in eq 4) obtained from simulations (red triangle) compared with published experimental data (black line),[23] the dielectric is IL [C_6mim][Tf_2N]. All of the results were carried out at V_{DS} = 0.1 V.

afford a conduction path established for electron transfer any more. Therefore, among all studied ILs, [C_6mim][BF_4] would exhibit the lowest possibility to form a conduction path on a-IGZO surface under the same gate voltage.

From the above analyses on IL-gated transistors at atomistic level, it is worth stating that one-dimensional analysis, such as number density distribution, potential distribution, and orientation distribution, can give the information of capacitance and averaged surface charge density, but it is not enough to clearly distinguish the difference of gating effect from different ILs, since the gating performance of IL-gated transistor is essentially dominated by not only how many charges could be induced but also how these charges would be distributed at a-IGZO surface (i.e., the 2D electric field distributions and surface charge densities).

In this work, the modeling for IL-gated transistor starts from the atomistic representation of the a-IGZO and ILs in MD simulations. Thus far, we could obtain the a-IGZO capacitance, EDL structure, the charge density across EDLs, and inhomogeneous charge distribution at semiconductor surface as well as the percolation-modeled conduction path(s) formed potentially for possible electron transfer. Analogous to heat transfer analysis via the resistance network analyses with the finite element method (FEM),[40,41] the detailed information at atomistic level was adopted to evaluate the macroscopic transfer characteristics of a real IL-gated transistor. Concretely, the MD-obtained local charge density at a-IGZO surface was taken as the input for the FEM analysis to quantitatively quantify the electrical conductance of the a-IGZO gated by IL-based EDLs, and the gate voltage (V_G) dependence of source−drain current (I_{DS}) in a real a-IGZO transistor could be derived to be compared with experimental results.

As shown in Figure 4a, the modeled a-IGZO (Figure 1b) has an area of 6.1 nm × 5.9 nm in xy-plane, with a uniform grid of 0.1 nm × 0.1 nm. Each grid has a specified electrical conductance derived from surface charge density

$$G_{grid} = \sigma_{2D}\mu_e \tag{1}$$

where μ_e is the carrier mobility of a-IGZO. After applying the boundary conditions and source−drain voltage (V_{DS}), I_{DS} can be calculated through the resistance network analysis by line integration of current density (eq S9). The detailed description of FEM analysis can be found in Part 8 of Supporting Information. Once I_{DS} through a-IGZO was acquired, the equivalent conductance of the overall a-IGZO ($G_{a\text{-IGZO}}$) could be computed by

$$G_{a\text{-IGZO}} = \frac{I_{DS}}{V_{DS}} \tag{2}$$

which is shown in Figure 4b. For ILs [$C_n$mim][Tf_2N] (n = 2, 4, 6, 10), it can be observed that the increase of alkyl chain length results in decreasing $G_{a\text{-IGZO}}$, consistent with the a-IGZO side capacitance values obtained by MD simulation. For IL [C_6mim][BF_4], although it can afford a larger EDL capacitance than [C_6mim][Tf_2N] at a-IGZO side, it provides the lowest $G_{a\text{-IGZO}}$, due to the most inhomogeneous charge distribution.

As $G_{a\text{-IGZO}} = \bar{\mu}\sigma\frac{W}{L}$, where $\frac{W}{L}$ is the width−length ratio of a-IGZO surface and has been given in simulation and $\bar{\mu}$ is the carrier mobility of the whole a-IGZO surface, which then can be calculated as

$$\bar{\mu} = \frac{G_{a\text{-IGZO}}}{\sigma} / \frac{W}{L} \tag{3}$$

If the overall a-IGZO is in metallic state, $\bar{\mu}$ would equal to μ_e. By comparing the difference between $\bar{\mu}$ and μ_e, a coefficient $\eta = \frac{\bar{\mu}}{\mu_e}$ was defined as homogeneity degree to quantitatively estimate the homogeneity of charge distribution, reflecting the effective carrier mobility of the overall a-IGZO surface. The closer the homogeneity degree is to 1, the more homogeneous and larger the conducting regions on a-IGZO surface would become, and the more metallic the a-IGZO surface could be. η for different ILs shows the same tendency as the equivalent conductance (Figure 4b), which implies that the inhomogeneous charge distribution has a significant impact on the carrier mobility of the semiconductor when using electrolytes as dielectrics. It is worthwhile to note that even though IL [C_6mim][BF_4] can induce a higher EDL capacitance at a-IGZO side, the current through the conduction path is the lowest when it was used as dielectric, owing to its EDL inducing the smallest homogeneity degree of 2D surface charge densities. $G_{a\text{-IGZO}}$ and η were also calculated under a gate voltage of 1.5 V (Figure S7), showing the same trend as 0.4 V.

With the obtained electrical conductance of a-IGZO gated by each IL, once can assess the transfer characteristics (the dependence of I_{DS} on V_G) of a real IL-gated transistor. For instance, the a-IGZO channel width (W') and length (L') were set as 50 and 20 μm, respectively, in experiments,[23] and the equivalent current should be

$$I'_{DS} = G_{a\text{-IGZO}}V_{DS}\frac{W'}{L'} / \frac{W}{L} \tag{4}$$

DOI: 10.1021/acsami.8b15199
ACS Appl. Mater. Interfaces 2018, 10, 43211−43218

Then, for IL [C_6mim][Tf_2N], when at V_{DS} = 0.1 V, the equivalent currents were computed as 0.0534, 0.718, and 6.68 μA at gate voltages of 0, 0.4, and 1.5 V, respectively, which agree well with the experimental results[23] both in trend and in magnitude (Figure 4c). Therefore, the gating characteristic at macroscopic level is successfully evaluated through the MD-obtained information at nanoscale. Certainly, this method could be tested by many of other types of ILs in further studies.

CONCLUSIONS

In summary, we investigated the EDL structure and charge distribution at different a-IGZO/ILs interfaces through MD simulations. It has demonstrated that ILs with different cations/anions formed diverse EDL structures at the a-IGZO surface and thus derived various EDL capacitances, which would induce different charge densities and distributions at a-IGZO surface. Besides surface charge density, the homogeneity of surface charge distribution is of paramount importance to the gating effect. By calculating the equivalent conductance of the whole a-IGZO surface, the gating effect was estimated directly, and the homogeneity degree of charge distribution was quantitatively delineated via the resistance network analysis. It strongly suggests that both charge density and homogeneity of charge distribution should be taken into account when estimating the gating effect of electrolyte-gated transistors. Also, the MD-obtained results could be taken as inputs to evaluate the macroscopic transfer characteristics of a real IL-gated transistor and show good agreement with experimental results.[23] That indicates that the hierarchical simulation approach, which combines MD simulation with resistance network analysis, could be used to investigate more types of ILs and then screen out better performed ILs for experiments and practical applications in future. However, although the capacitance and homogeneity of charge distribution were successfully described, the relationship between them is still not fully understood and requires more work to determine their interactions. The ion size effect on the transfer characteristic of metal-oxide semiconductor revealed by simulation in this work also calls more experimental verifications.

METHODS

Molecular Dynamics Simulation. The a-IGZO used in MD simulation was obtained from crystalline IGZO by quenched molecular dynamics (QMD), and details can be found in Part 1 of Supporting Information. As shown in Figure 1b, a channel-like MD system consists of a slab of ILs enclosed between Au(111) and a-IGZO electrodes with an area of 6.1 nm × 5.9 nm parallel to the electrode surface. By analyzing the radius of ion gyration (Table S1), such a surface area is confirmed to be large enough for modeling the EDL structure formed between IL and solid interfaces. It also can be seen that in literature similar surface size has already been used to analyze properties of EDL.[42−44] The a-IGZO surface is separated from gold surface by 8.0 nm, which is wide enough to prevent overlapping of the EDLs formed at both electrodes and produce a bulklike IL region in the middle of system, as revealed by density distributions plotted along the whole z-direction in Figure S3. The gate voltage applied between the gold and a-IGZO was maintained using the constant potential method during the MD simulations.[45] Through the constant potential method, the potential on the electrode surfaces was same everywhere and located at a plane across the center of surface atoms. It has been proved that this method can take into account the electronic polarizability of the electrode surfaces.[46,47] A nonpolarizable all-atom model was used for all five different ionic liquids ([$C_n$mim][Tf_2N] (n = 2, 4, 6, 10) and [C_6mim][BF_4]),[48] and the force fields for electrodes were taken from ref 49 for a-IGZO and ref 50 for gold. These nonpolarizable force fields for ILs, which can significantly decrease the computational consuming, have been widely tested by other researchers and have also been used to analyze the EDL properties.[43,51,52] Note that the potential applied between the gold and a-IGZO surfaces does not include the potential drop across a-IGZO. Therefore, a gate voltage, 0.4 V, was chosen to apply in MD simulation to simulate an intermediate state of a gate voltage between 0.4 and 1.0 V in experiments; detailed information of chosen gate voltage can be found in Part 2 of Supporting Information.

MD simulations were performed via a customized GROMACS code,[53] with a time step of 1 fs. LINCS algorithm is used to constrain chemical bonds, including H-atom.[54] To accelerate the ion moving and save computational resources, the temperature of IL was maintained at 393 K using the Nosé−Hoover thermostat, which is below the decomposition temperature of ILs studied in this work.[55−57] The number of IL molecules inside the channel was tuned to make the ILs in central part of the channel showed a bulklike state. The particle mesh Ewald method was used to compute the electrostatic interactions.[45] An fast Fourier transform (FFT) grid spacing of 0.1 nm and cubic interpolation for charge distribution were used to compute the electrostatic interactions in the reciprocal space. The cutoff for both Coulombic and van der Waals interactions is 1.1 nm. Each simulation was run for 10 ns to reach equilibrium, and then a 50 ns production run was performed for analysis.

Resistant Network Analysis. To calculate the current, the a-IGZO surface was considered as a periodical material with a unit cell, which consists of 3599 grids (61 × 59), each grid has a different electrical conductance, which is derived from surface charge density. The size of grid (0.1 nm × 0.1 nm) is equal to the FFT grid spacing used in MD simulation, which means that this resolution could inherit the MD results without loss of precision. Moreover, the effect of the grid size on the accuracy of results was verified by applying a smaller gird size, which generated very similar results compared with the large one (Figure S10). A bias potential with 0.1 V was applied along y-axis (potential along x-axis was also tested, which shows the similar results; see Part 9 of Supporting Information), equipotential boundary condition was used at x = 0 and 6.1 nm. The current can be derived by the line integration of current density along the vector, which is perpendicular to the direction of the electric field. All these calculations were carried out by FEM. The detailed information can be found in Supporting Information.

ASSOCIATED CONTENT

Supporting Information

The Supporting Information is available free of charge on the ACS Publications website at DOI: 10.1021/acsami.8b15199.

Generation of amorphous $InGaZnO_4$ structure; relationship between gate voltage and potential; radius of gyration of ions and density profiles of [C_{10}mim][Tf_2N] along the whole z-direction; gate side capacitance; 2D surface charge distribution at a-IGZO surface; details of percolation visualization; equivalent conductance and effective mobility at 1.5 V; finite element method; the equivalent conductance and homogeneity degree as the bias potential was applied along x-axis; a denser grid tested for FEM calculation (PDF)

AUTHOR INFORMATION

Corresponding Author

*E-mail: gfeng@hust.edu.cn.

ORCID

Nina Balke: 0000-0001-5865-5892

Philip D. Rack: 0000-0002-9964-3254

DOI: 10.1021/acsami.8b15199
ACS Appl. Mater. Interfaces 2018, 10, 43211−43218

Thomas Zac Ward: 0000-0002-1027-9186
Sergei V. Kalinin: 0000-0001-5354-6152
Sheng Dai: 0000-0002-8046-3931
Guang Feng: 0000-0001-6659-9181

Author Contributions

[▽]W.Z. and S.B. contributed equally to this work.

Notes

The authors declare no competing financial interest.

■ ACKNOWLEDGMENTS

This work was financially supported by the National Natural Science Foundation of China (51876072) and Shenzhen Basic Research Project (JCYJ20170307171511292). All simulations were performed at the National Supercomputing Centers in Tianjin (Tianhe-1A) and Guangzhou (Tianhe II). T.Z.W., N.B. and S.V.K. thank the support by the Division of Materials Sciences and Engineering, Basic Energy Sciences, Department of Energy. P.D.R. acknowledges funding for the transistor device fabrication from NSF grant 1544686, which was partially fabricated at the Center for Nanophase Materials Sciences, which is a DOE office of Science user facility. S.D. was supported by the Fluid Interface Reactions, Structures & Transport, an Energy Frontier Research Center—US Department of Energy, Office of Science, Office of Basic Energy Sciences.

■ REFERENCES

(1) Panzer, M. J.; Frisbie, C. D. Polymer Electrolyte Gate Dielectric Reveals Finite Windows of High Conductivity in Organic Thin Film Transistors at High Charge Carrier Densities Polymer Electrolyte Gate Dielectric Reveals Finite Windows of High. *J. Am. Chem. Soc.* **2005**, *127*, 6960−6961.
(2) Ueno, K.; Nakamura, S.; Shimotani, H.; Ohtomo, A.; Kimura, N.; Nojima, T.; Aoki, H.; Iwasa, Y.; Kawasaki, M. Electric-Field-Induced Superconductivity in an Insulator. *Nat. Mater.* **2008**, *7*, 855−858.
(3) Ye, J. T.; Inoue, S.; Kobayashi, K.; Kasahara, Y.; Yuan, H. T.; Shimotani, H.; Iwasa, Y. Liquid-Gated Interface Superconductivity on an Atomically Flat Film. *Nat. Mater.* **2010**, *9*, 125−128.
(4) Ueno, K.; Nakamura, S.; Shimotani, H.; Yuan, H. T.; Kimura, N.; Nojima, T.; Aoki, H.; Iwasa, Y.; Kawasaki, M. Discovery of Superconductivity in $KTaO_3$ by Electrostatic Carrier Doping. *Nat. Nanotechnol.* **2011**, *6*, 408−412.
(5) Ji, H.; Wei, J.; Natelson, D. Modulation of the Electrical Properties of VO_2 Nanobeams Using an Ionic Liquid as a Gating Medium. *Nano Lett.* **2012**, *12*, 2988−2992.
(6) Nakano, M.; Shibuya, K.; Okuyama, D.; Hatano, T.; Ono, S.; Kawasaki, M.; Iwasa, Y.; Tokura, Y. Collective Bulk Carrier Delocalization Driven by Electrostatic Surface Charge Accumulation. *Nature* **2012**, *487*, 459−462.
(7) Jeong, J.; Aetukuri, N.; Graf, T.; Schladt, T. D.; Samant, M. G.; Parkin, S. S. P. Suppression of Metal-Insulator Transition in VO_2 by Electric Field-Induced Oxygen Vacancy Formation. *Science* **2013**, *339*, 1402−1405.
(8) Kim, S. H.; Hong, K.; Lee, K. H.; Frisbie, C. D. Performance and Stability of Aerosol-Jet-Printed Electrolyte-Gated Transistors Based on Poly(3-Hexylthiophene). *ACS Appl. Mater. Interfaces* **2013**, *5*, 6580−6585.
(9) Scherwitzl, R.; Zubko, P.; Lezama, I. G.; Ono, S.; Morpurgo, A. F.; Catalan, G.; Triscone, J. M. Electric-Field Control of the Metal-Insulator Transition in Ultrathin $NdNiO_3$ Films. *Adv. Mater.* **2010**, *22*, 5517−5520.
(10) Asanuma, S.; Xiang, P. H.; Yamada, H.; Sato, H.; Inoue, I. H.; Akoh, H.; Sawa, A.; Ueno, K.; Shimotani, H.; Yuan, H.; Kawasaki, M.; Iwasa, Y. Tuning of the Metal-Insulator Transition in Electrolyte-Gated $NdNiO_3$ Thin Films. *Appl. Phys. Lett.* **2010**, *97*, No. 142110.
(11) Lee, Y.; Clement, C.; Hellerstedt, J.; Kinney, J.; Kinnischtzke, L.; Leng, X.; Snyder, S. D.; Goldman, A. M. Phase Diagram of Electrostatically Doped $SrTiO_3$. *Phys. Rev. Lett.* **2011**, *106*, No. 136809.
(12) Bollinger, A. T.; Dubuis, G.; Yoon, J.; Pavuna, D.; Misewich, J.; Božović, I. Superconductor−Insulator Transition in $La_{2-X}Sr_xCuO_4$ at the Pair Quantum Resistance. *Nature* **2011**, *472*, 458−460.
(13) Thiemann, S.; Gruber, M.; Lokteva, I.; Hirschmann, J.; Halik, M.; Zaumseil, J. High-Mobility ZnO Nanorod Field-Effect Transistors by Self-Alignment and Electrolyte-Gating. *ACS Appl. Mater. Interfaces* **2013**, *5*, 1656−1662.
(14) Perera, M. M.; Lin, M.-W.; Chuang, H.-J.; Chamlagain, B. P.; Wang, C.; Tan, X.; Cheng, M. M.-C.; Tománek, D.; Zhou, Z. Improved Carrier Mobility in Few-Layer MoS_2 Field-Effect Transistors with Ionic-Liquid Gating. *ACS Nano* **2013**, *7*, 4449−4458.
(15) Chuang, H. J.; Tan, X.; Ghimire, N. J.; Perera, M. M.; Chamlagain, B.; Cheng, M. M. C.; Yan, J.; Mandrus, D.; Tománek, D.; Zhou, Z. High Mobility WSe_2 P- and N- Field-Effect Transistors Contacted by Highly Doped Graphene for Low-Resistance Contacts. *Nano Lett.* **2014**, *14*, 3594−3601.
(16) Misra, R.; McCarthy, M.; Hebard, A. F. Electric Field Gating with Ionic Liquids. *Appl. Phys. Lett.* **2007**, *90*, No. 052905.
(17) Park, S.; Lee, S.; Kim, C.-H.; Lee, I.; Lee, W.-J.; Kim, S.; Lee, B.-G.; Jang, J.-H.; Yoon, M.-H. Sub-0.5 V Highly Stable Aqueous Salt Gated Metal Oxide Electronics. *Sci. Rep.* **2015**, *5*, No. 13088.
(18) Pudasaini Pushpa, R.; Noh Joo, H.; Wong Anthony, T.; Ovchinnikova Olga, S.; Haglund Amanda, V.; Dai, S.; Ward Thomas, Z.; Mandrus, D.; Rack Philip, D. Ionic Liquid Activation of Amorphous Metal-Oxide Semiconductors for Flexible Transparent Electronic Devices. *Adv. Funct. Mater.* **2016**, *26*, 2820−2825.
(19) Ono, S.; Miwa, K.; Seki, S.; Takeya, J. A Comparative Study of Organic Single-Crystal Transistors Gated with Various Ionic-Liquid Electrolytes. *Appl. Phys. Lett.* **2009**, *94*, No. 063301.
(20) Xia, Y.; Cho, J. H.; Lee, J.; Ruden, P. P.; Frisbie, C. D. Comparison of the Mobility-Carrier Density Relation in Polymer and Single-Crystal Organic Transistors Employing Vacuum and Liquid Gate Dielectrics. *Adv. Mater.* **2009**, *21*, 2174−2179.
(21) Lee, E.; Ko, J.; Lim, K. H.; Kim, K.; Park, S. Y.; Myoung, J. M.; Kim, Y. S. Gate Capacitance-Dependent Field-Effect Mobility in Solution-Processed Oxide Semiconductor Thin-Film Transistors. *Adv. Funct. Mater.* **2014**, *24*, 4689−4697.
(22) Zhu, W.; Low, T.; Lee, Y. H.; Wang, H.; Farmer, D. B.; Kong, J.; Xia, F.; Avouris, P. Electronic Transport and Device Prospects of Monolayer Molybdenum Disulphide Grown by Chemical Vapour Deposition. *Nat. Commun.* **2014**, *5*, No. 3087.
(23) Pudasaini, P. R.; Noh, J. H.; Wong, A.; Haglund, A. V.; Dai, S.; Ward, T. Z.; Mandrus, D.; Rack, P. D. Ionic Liquid Versus SiO_2 Gated a-IGZO Thin Film Transistors: A Direct Comparison. *ECS J. Solid State Sci. Technol.* **2015**, *4*, Q105−Q109.
(24) Lockett, V.; Sedev, R.; Ralston, J.; Horne, M.; Rodopoulos, T. Differential Capacitance of the Electrical Double Layer in Imidazolium-Based Ionic Liquids: Influence of Potential, Cation Size, and Temperature. *J. Phys. Chem. C* **2008**, *112*, 7486−7495.
(25) Lockett, V.; Horne, M.; Sedev, R.; Rodopoulos, T.; Ralston, J. Differential Capacitance of the Double Layer at the Electrode/Ionic Liquids Interface. *Phys. Chem. Chem. Phys.* **2010**, *12*, 12499.
(26) Liu, X.; Wang, Y.; Li, S.; Yan, T. Effects of Anion on the Electric Double Layer of Imidazolium-Based Ionic Liquids on Graphite Electrode by Molecular Dynamics Simulation. *Electrochim. Acta* **2015**, *184*, 164−170.
(27) Jo, S.; Park, S. W.; Shim, Y.; Jung, Y. J. Effects of Alkyl Chain Length on Interfacial Structure and Differential Capacitance in Graphene Supercapacitors: A Molecular Dynamics Simulation Study. *Electrochim. Acta* **2017**, *247*, 634−645.
(28) Kim Se, H.; Hong, K.; Xie, W.; Lee Keun, H.; Zhang, S.; Lodge Timothy, P.; Frisbie, C. D. Electrolyte-Gated Transistors for Organic and Printed Electronics. *Adv. Mater.* **2013**, *25*, 1822−1846.

DOI: 10.1021/acsami.8b15199
ACS Appl. Mater. Interfaces 2018, 10, 43211−43218

(29) Black, J. M.; Come, J.; Bi, S.; Zhu, M.; Zhao, W.; Wong, A. T.; Noh, J. H.; Pudasaini, P. R.; Zhang, P.; Okatan, M. B.; Dai, S.; Kalinin, S. V.; Rack, P. D.; Ward, T. Z.; Feng, G.; Balke, N. Role of Electrical Double Layer Structure in Ionic Liquid Gated Devices. *ACS Appl. Mater. Interfaces* **2017**, *9*, 40949−40958.
(30) Xia, Y.; Xie, W.; Ruden, P. P.; Frisbie, C. D. Carrier Localization on Surfaces of Organic Semiconductors Gated with Electrolytes. *Phys. Rev. Lett.* **2010**, *105*, No. 036802.
(31) Li, M.; Graf, T.; Schladt, T. D.; Jiang, X.; Parkin, S. S. P. Role of Percolation in the Conductance of Electrolyte-Gated $SrTiO_3$. *Phys. Rev. Lett.* **2012**, *109*, No. 196803.
(32) Mezger, M.; Schroder, H.; Reichert, H.; Schramm, S.; Okasinski, J. S.; Schoder, S.; Honkimaki, V.; Deutsch, M.; Ocko, B. M.; Ralston, J.; Rohwerder, M.; Stratmann, M.; Dosch, H. Molecular Layering of Fluorinated Ionic Liquids at a Charged Sapphire (0001) Surface. *Science* **2008**, *322*, 424−428.
(33) Walker, D. A.; Kowalczyk, B.; de la Cruz, M. O.; Grzybowski, B. A. Electrostatics at the Nanoscale. *Nanoscale* **2011**, *3*, 1316.
(34) Lang, A. C.; Sloppy, J. D.; Ghassemi, H.; Devlin, R. C.; Sichel-Tissot, R. J.; Idrobo, J.-C.; May, S. J.; Taheri, M. L. Atomic-Scale Characterization of Oxide Thin Films Gated by Ionic Liquid. *ACS Appl. Mater. Interfaces* **2014**, *6*, 17018−17023.
(35) Hu, G.; Pandey, G. P.; Liu, Q.; Anaredy, R. S.; Ma, C.; Liu, M.; Li, J.; Shaw, S. K.; Wu, J. Self-Organization of Ions at the Interface between Graphene and Ionic Liquid Deme-TFSI. *ACS Appl. Mater. Interfaces* **2017**, *9*, 35437−35443.
(36) Körner, W.; Urban, D. F.; Elsässer, C. Origin of Subgap States in Amorphous In-Ga-Zn-O. *J. Appl. Phys.* **2013**, *114*, No. 163704.
(37) Nomura, K.; Kamiya, T.; Ohta, H.; Uruga, T.; Hirano, M.; Hosono, H. Local Coordination Structure and Electronic Structure of the Large Electron Mobility Amorphous Oxide Semiconductor In-Ga-Zn-O: Experiment and ab initio Calculations. *Phys. Rev. B* **2007**, *75*, No. 035212.
(38) Yuyama, K.; Masuda, G.; Yoshida, H.; Sato, T. Ionic Liquids Containing the Tetrafluoroborate Anion Have the Best Performance and Stability for Electric Double Layer Capacitor Applications. *J. Power Sources* **2006**, *162*, 1401−1408.
(39) Nomura, K.; Ohta, H.; Takagi, A.; Kamiya, T.; Hirano, M.; Hosono, H. Room-Temperature Fabrication of Transparent Flexible Thin-Film Transistors Using Amorphous Oxide Semiconductors. *Nature* **2004**, *432*, 488−492.
(40) Guo, Z.-Y.; Zhu, H.-Y.; Liang, X.-G. Entransy—a Physical Quantity Describing Heat Transfer Ability. *Int. J. Heat Mass Transfer* **2007**, *50*, 2545−2556.
(41) Wang, K.; Zhang, L.; Ji, B.; Yuan, J. The Thermal Analysis on the Stackable Supercapacitor. *Energy* **2013**, *59*, 440−444.
(42) Vatamanu, J.; Borodin, O.; Smith, G. D. Molecular Insights into the Potential and Temperature Dependences of the Differential Capacitance of a Room-Temperature Ionic Liquid at Graphite Electrodes. *J. Am. Chem. Soc.* **2010**, *132*, 14825−14833.
(43) Sha, M.; Dou, Q.; Luo, F.; Zhu, G.; Wu, G. Molecular Insights into the Electric Double Layers of Ionic Liquids on Au(100) Electrodes. *ACS Appl. Mater. Interfaces* **2014**, *6*, 12556−12565.
(44) Yu, Z.; Fang, C.; Huang, J.; Sumpter, B. G.; Qiao, R. Solvate Ionic Liquids at Electrified Interfaces. *ACS Appl. Mater. Interfaces* **2018**, *10*, 32151−32161.
(45) Raghunathan, A. V.; Aluru, N. R. Self-Consistent Molecular Dynamics Formulation for Electric-Field-Mediated Electrolyte Transport through Nanochannels. *Phys. Rev. E* **2007**, *76*, No. 011202.
(46) Wu, P.; Huang, J.; Meunier, V.; Sumpter, B. G.; Qiao, R. Complex Capacitance Scaling in Ionic Liquids-Filled Nanopores. *ACS Nano* **2011**, *5*, 9044−9051.
(47) Kondrat, S.; Wu, P.; Qiao, R.; Kornyshev, A. A. Accelerating Charging Dynamics in Subnanometre Pores. *Nat. Mater.* **2014**, *13*, 387−393.
(48) Canongia Lopes, J. N.; Pádua, A. A. Molecular Force Field for Ionic Liquids Composed of Triflate or Bistriflylimide Anions. *J. Phys. Chem. B* **2004**, *108*, 16893−16898.
(49) Rappé, A. K.; Casewit, C. J.; Colwell, K.; Goddard Iii, W.; Skiff, W. Uff, a Full Periodic Table Force Field for Molecular Mechanics and Molecular Dynamics Simulations. *J. Am. Chem. Soc.* **1992**, *114*, 10024−10035.
(50) Verde, A. V.; Acres, J. M.; Maranas, J. K. Investigating the Specificity of Peptide Adsorption on Gold Using Molecular Dynamics Simulations. *Biomacromolecules* **2009**, *10*, 2118−2128.
(51) Paek, E.; Pak, A. J.; Hwang, G. S. A Computational Study of the Interfacial Structure and Capacitance of Graphene in [Bmim][PF_6] Ionic Liquid. *J. Electrochem. Soc.* **2013**, *160*, A1−A10.
(52) Wang, S.; Li, S.; Cao, Z.; Yan, T. Molecular Dynamic Simulations of Ionic Liquids at Graphite Surface. *J. Phys. Chem. C* **2010**, *114*, 990−995.
(53) Hess, B.; Kutzner, C.; van der Spoel, D.; Lindahl, E. Gromacs 4: Algorithms for Highly Efficient, Load-Balanced, and Scalable Molecular Simulation. *J. Chem. Theory Comput.* **2008**, *4*, 435−447.
(54) Hess, B.; Bekker, H.; Berendsen, H. J.; Fraaije, J. G. Lincs: A Linear Constraint Solver for Molecular Simulations. *J. Comput. Chem.* **1997**, *18*, 1463−1472.
(55) Huddleston, J. G.; Visser, A. E.; Reichert, W. M.; Willauer, H. D.; Broker, G. A.; Rogers, R. D. Characterization and Comparison of Hydrophilic and Hydrophobic Room Temperature Ionic Liquids Incorporating the Imidazolium Cation. *Green Chem.* **2001**, *3*, 156−164.
(56) Maton, C.; De Vos, N.; Stevens, C. V. Ionic Liquid Thermal Stabilities: Decomposition Mechanisms and Analysis Tools. *Chem. Soc. Rev.* **2013**, *42*, 5963−5977.
(57) Kulkarni, P. S.; Branco, L. C.; Crespo, J. G.; Nunes, M. C.; Raymundo, A.; Afonso, C. A. M. Comparison of Physicochemical Properties of New Ionic Liquids Based on Imidazolium, Quaternary Ammonium, and Guanidinium Cations. *Chem. - Eur. J.* **2007**, *13*, 8478−8488.

DOI: 10.1021/acsami.8b15199
ACS Appl. Mater. Interfaces 2018, 10, 43211−43218